

Epitaxially strained SnTiO₃ at finite temperatures

D. Wang,^{1,*} L. Liu,^{2,†} J. Liu,³ and N. Zhang⁴

¹*School of Microelectronics and State Key Laboratory for Mechanical Behaviour of Materials, Xi'an Jiaotong University, Xi'an 710049, China*

²*College of Materials Science and Engineering, Guilin University of Technology, Guilin, 541004, China*

³*State Key Laboratory for Mechanical Behavior of Materials,*

School of Materials Science and Engineering, Xi'an Jiaotong University, Xi'an, China, 710049

⁴*Electronic Materials Research Laboratory-Key Laboratory of the Ministry of Education and International Centre for Dielectric Research, Xi'an Jiaotong University, Xi'an 710049, China*

We obtain the phase diagram of SnTiO₃ with respect to epitaxial strain and temperature. Combining effective Hamiltonian and direct *ab initio* computation, we demonstrate the complex features of the phase diagram and provide insight into the epitaxially strained SnTiO₃, a presumably “simple” perovskite. For instance, the *P4mm* to *Amm2* phase transition via the *Cm* phase, with increasing epitaxial strain. In addition, two triple points are found, which may be exploited to achieve high-performance piezoelectric effects. Finally, by epitaxial strain control, it is shown that the SnTiO₃ can be modified from hard to soft ferroelectrics.

I. INTRODUCTION

Piezoelectricity is a phenomenon in certain materials that strain and electric polarisation can induce and/or influence each other. Ferroelectric materials, which are inherently piezoelectric, can produce an electric polarisation proportional to the load, in response to an applied mechanical strain. Similarly, such materials will produce a mechanical deformation (strain) in response to an applied voltage. Switchable polarisation makes ferroelectrics a critical component in memories, actuators, electro-optic devices, and potential candidates for nanoelectronics¹.

In recent years, it has been found that materials of high-performance piezoelectricity are often associated with morphotropic boundary (MPB), with examples including Pb(Zr,Ti)O₃² and (K,Na)NbO₃-LiTaO₃-LiSbO₃³, or triple points, e.g. in (Ba,Ca)(Zr,Ti)O₃⁴. Such phase boundaries and tricritical points are created by engineering solid solutions to a certain composition, where the crystal structure changes abruptly and the piezoelectric properties are maximal. There are three important situations that have been extensively studied: (i) MPB in pure perovskites that separates regions of tetragonal from rhombohedral symmetry⁵; (ii) MPB formed in perovskites dissolved with a small amount of non-perovskite-structured materials that can cause lattice distortions³; (iii) Regions close to a triple point where cubic paraelectric phase (C), ferroelectric rhombohedral (R), and tetragonal (T) phases meet⁴. In addition, another important method to engineer desired ferroelectric materials is epitaxial thin-film growth and the introduction of intrinsic lattice strain. Epitaxial films are of great importance for highly integrated design and intelligent control technology^{6,7}. Strain engineering has been widely adopted to tune the large *2p-3d* charge hybridisation between the strongly correlated *3d* electrons in transition metal ions and *2p* electrons of oxygens⁸⁻¹¹. For instance, both compressive and tensile strains increase the Ni *3d* band width and favour the metallic phase in NdNiO₃¹². In addition, substrate clamping will force the temperature dependence of in-plane lattice parameters of films to follow that of the substrates, which may lead to unexpected phase transitions and domain formation in epitaxial films¹³. Therefore,

strain constraint as an attractive method to fine tuning properties of films, can even introduce multi-phase coexistence in thin films.

Nowadays commonly used high-performance piezoelectric materials, including PbTiO₃ and Pb(Mn,Nb)O₃, contain hazardous lead (Pb). Since Pb is harmful to environment and human health, lead-free ferroelectric materials are highly desired. Many lead-free materials are based on (Bi_{0.5},Na_{0.5})TiO₃, (K,Na)NbO₃ or BaTiO₃, however, their performance is still sub-optimal compared to Pb-containing materials¹⁴. Since Sn and Pb belong to the same family, SnTiO₃ is expected to achieve high-performance piezoelectricity with environmentally benign elements¹⁵. Indeed, it has been shown that SnTiO₃ has large polarisation and large axial ratio^{16,17}, even larger than PbTiO₃, which makes it a promising candidate. But for various reasons, SnTiO₃ bulk material was still unavailable so far, mainly due to the fact that Sn²⁺ is easy to become Sn⁴⁺, and Sn is prone to enter into the B site (where Ti ion stays) due to its small ionic radius. However, researchers continued to look for opportunities of exploiting the remarkable properties of SnTiO₃. For instance, Xie *et al* considered Sn-doped BaTiO₃¹⁸, Bennett *et al* considered Sn(Al_{0.5},Nb_{0.5})O₃¹⁹, while Suzuki *et al* obtained Sn-doped SrTiO₃²⁰, and Laurita investigated (Sr,Sn)TiO₃ and (Ba,Ca,Sn)TiO₃²¹.

In addition to experimental work, there are also many theoretical investigations on SnTiO₃^{15,17,22-26}. In previous theoretical investigations, however, most are based on direct *ab initio* computation, which cannot provide information regarding SnTiO₃ at finite temperatures. Therefore, important questions remain unanswered. For instance, what are the conditions for the existence of different ferroelectric phases? How is the phase diagram of SnTiO₃ like? Can such a seemingly simple perovskite (SnTiO₃ is not made of solid solution) possess complex features? In this work, we will focus on finite temperature properties of epitaxially strained SnTiO₃ and address these important questions. We note that such information will be useful for the fabrication of SnTiO₃ bulk, or the growth of SnTiO₃ film, and engineering excellent ferroelectric materials containing SnTiO₃. Moreover, via first-principles-based effective Hamiltonian approach and direct *ab initio* calculations, we show that SnTiO₃ has a rather complex phase diagram un-

der epitaxial strains, containing interesting phase boundaries and triple points.

II. METHOD

We employ the effective Hamiltonian approach combined with Monte-Carlo simulation to obtain finite temperature properties SnTiO₃. The effective Hamiltonian used here was originally developed in Ref.²⁷, which incorporates the coupled dynamics of the soft mode, strain, and dipole interactions. Its internal energy is given by

$$E = E^{\text{FE}}(\{\mathbf{u}_i\}, \{\mathbf{v}_i\}, \eta_H),$$

where \mathbf{u}_i is the local soft-mode in unit cell i , and is proportional to the local electric dipole moment in that cell, when multiplied by Born effective charge. We note that \mathbf{u}_i here is located on the A-site (where Sn stays), and represents the collective motion of Sn, Ti, and O atoms inside one unit cell. The \mathbf{v}_i are Sn-centered local displacements related to the inhomogeneous strain inside each unit cell. η_H is the homogeneous strain tensor. The energy terms and associated parameters can be found in Ref.²⁸. In this work, we extended the effective Hamiltonian and expanded the local energy term to 8th order (similar to Ref.²⁹) in order to describe the internal energy more precisely³⁰. In addition, the antiferro-distortive (AFD) oxygen octahedron tilting is also considered with the energy term being³¹

$$E = E^{\text{AFD}}(\{\omega_i\}, \{\mathbf{u}_i\}, \{\mathbf{v}_i\}, \eta_H),$$

where the new variable ω_i represents the oxygen tilting in unit cell i , and centres on the B-site atom (i.e., Ti). The energy term E^{AFD} also includes the couplings between AFD, and all the other dynamical variables. The associated parameters in E^{AFD} are obtained in a similarly way as Ref.^{28,32}.

With the effective Hamiltonian, we perform Monte-Carlo simulation on a $12 \times 12 \times 12$ supercell, containing 8640 atoms. The system is set to meet the periodic boundary condition along the (pseudo) x, y, z direction, and subject to various epitaxial strain. In each simulation at a given epitaxial strain misfit s , we gradually cool down the system from 2500 K down to 5 K. For each temperature, we carry out 160,000 Monte Carlo steps to obtain averaged physical quantities, most importantly, the supercell average of local mode, which can be used to determine the symmetry of the system and the approximate positions of each atom in it.

We have also performed direct *ab initio* computation to corroborate first-principles-based Monte-Carlo simulation results. For this purpose, the open source ABINIT software package cite³³ is used along with the local density approximation (LDA)³⁴ and the projector-augmented-wave (PAW) method³⁵. We use the pseudo-potentials implemented in the GBRV package³⁶, and the Sn $4d\ 5s\ 5p$, Ti $3s\ 3p\ 4s\ 3d$, and O $2s\ 2p$ orbitals are treated as valence orbitals. For convergence, we have chosen the cut-off energy (*ecut*) to be 25 Hartree (1 Hartree = 27.211 eV) for plane wave expansion, and fine grid of the cut-off energy (*pawcutdg*) is selected to be ~ 50 Hartree in all calculations. In addition, k -point sampling of $6 \times 6 \times 6$ Monkhorst-Pack grid³⁷ was used. The atomic coordinates are relaxed until all atomic-force components are smaller than 10^{-5} Ha/Bohr, and the cell size and shape are varied until all stress components are below 10^{-7} Htree/Bohr³.

III. RESULTS AND DISCUSSION

A. Phase transitions and phase diagram

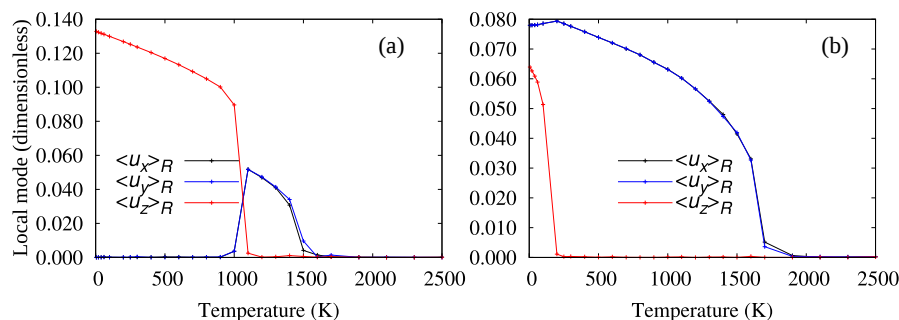


FIG. 1: Polarization versus temperature at two given strain misfit, $s = 0.375\%$ (Left panel) and $s = 1\%$ (Right panel).

We first obtain the supercell averaged local mode versus

temperature of SnTiO₃ under various tensile epitaxial strains,

which is expected to be able to stabilise SnTiO_3 ¹⁷. Such information enables us to find the evolution of structural phases with respect to temperature and epitaxial strain, and more importantly, the phase transition temperatures of the system. Figure 1 shows the results with epitaxial strain $s = 0.375\%$ and $s = 1\%$ ⁴⁹. For the smaller epitaxial strain $s = 0.375\%$, the system adopts $P4mm$ phase for temperature $T \lesssim 1000$ K, ($P_x = P_y = 0, P_z > 0$), as temperature increases it undergoes a phase transition to become the $Amm2$ phase ($P_x = P_y > 0, P_z = 0$), and eventually adopts the cubic phase for $T \gtrsim 1500$ K. The whole process is a little similar to that of BaTiO_3 and $(\text{Na}_{0.5}\text{K}_{0.5})\text{NbO}_3$, where several structural phases are involved in phase transitions. Here, however, a rather drastic change happens at around 1000 K as the polarisation rotates from out-of-plane to the in-plane configuration. For the larger epitaxial strain ($s = 1\%$), there are also two phase transitions. At low temperature ($T \lesssim 197$ K), it adopts the Cm ($P_x = P_y > 0, P_z > 0$) phase, which changes to the $P4mm$ phase as temperature increases, and finally become paraelectric at $T \simeq 1750$ K. It is worth noting that no correlated AFD tilting of oxygen octahedron was

observed for the epitaxial strains investigated here, which are consistent with previous known results^{17,50}. Figure 1 indicates that four phases (paraelectric $Pm\bar{3}m$, orthorhombic $Amm2$, tetragonal $P4mm$, and monoclinic Cm) phase can all exist in SnTiO_3 at proper temperature and epitaxial strain. Consistent with previous results²⁸, without strain constraint or at very small strain ($s < 0.5\%$, see Fig. 2), the system adopts the $P4mm$ phase ($P_z > 0, P_{x,y} = 0$) at low temperature, and only has one phase transition ($P4mm$ to paraelectric) as temperature increases. Interestingly, Figure 1(b) shows a region ($T \leq 200$ K) that corresponds to the M_B phase (belong to space group Cm)^{30,38}, and for smaller s (e.g., at $s = 0.75\%$), we have observed that $P_z > P_x = P_y$, which is also Cm , but corresponds to the M_A phase³⁸. Moreover, in Figure 1(a), both M_A and M_B phases exist between the T ($P4mm$) and O ($Amm2$) phases. The phase transition sequence is similar to the local structure evolution of $\text{Pb}(\text{Ti}_{1-x}\text{Zr}_x)\text{O}_3$ with increasing x ³⁹. We note that such monoclinic region has been shown to play critical role in high-performance piezoelectric materials⁴⁰.

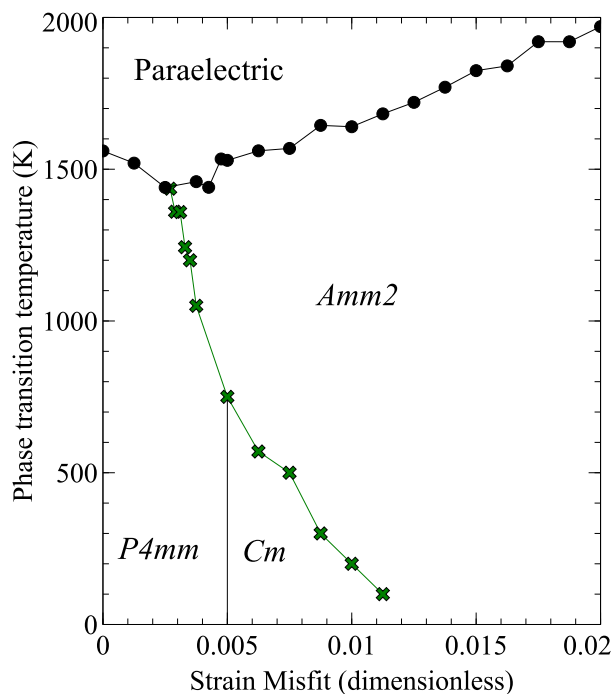


FIG. 2: Phase diagram of epitaxially strained SnTiO_3 .

We now turn to the phase diagram of SnTiO_3 with respect to temperature and epitaxial strain. To this end, we performed simulations similar to that of Fig. 1 at different epitaxial strains and obtained the results shown in Fig. 2,

which demonstrates several important features. First, for all the investigated strain misfit (up to 2%), Fig. 2 shows that SnTiO_3 undergoes a paraelectric to ferroelectric phase transition at rather high temperature ($T_C > 1400$ K). The reason

for the high T_C is likely due to the large intrinsic spontaneous polarisation, which was discussed in a previous work²⁸. Second, T_C initially decreases with s , reaching a minimum, and then increases again⁴¹, the lowest point corresponds to a triple point separating the paraelectric phase and the other two ferroelectric phases (tetragonal $P4mm$ and orthorhombic $Amm2$), similar to what happens in ultrathin $PbTiO_3$ films⁴². Third, for a small region ($0.5\% < s < 1\%$), there exists the Cm phase ($P_x = P_y > 0, P_z > 0, P_x \neq P_z$), which separates the $P4mm$ and $Amm2$ phases and acts as a bridge that makes the rotation from the in-plane polarisation to out-of-plane easy. We note that the existence of the Cm phase is consistent with results obtained in Ref.¹⁷.

We note that the first triple point in Fig. 2, where one paraelectric cubic phase and two ferroelectric phases converge, is a good place to look for giant piezoelectric effects in lead-free materials. For instance, such triple point was found and exploited in binary compounds including $(Ba_{0.7}, Ca_{0.3})TiO_3$ - $Ba(Zr_{0.2}, Ti_{0.8})O_3$ (BCZT)⁴, $Ba(Sn_{0.12}, Ti_{0.88})O_3$ - $x(Ba_{0.7}, Ca_{0.3})O_3$ ⁴³, and other $BaTiO_3$ -derived systems⁴⁴. More importantly, a second triple point exists, where three ferroelectric phases ($P4mm$, $Amm2$, and Cm) converge. There are three boundaries around this point. The boundary at $s = 0.5\%$ separates the $P4mm$ and the Cm phase, resembling the MPB seen in $Pb(Zr_{1-x}, Ti_x)O_3$, in which two different structural phases exist with a buffer region at $x \simeq 0.48$. In $Pb(Zr_{1-x}, Ti_x)O_3$ the monoclinic phase serves as a bridge between the higher symmetry tetragonal phase (with [001] polarisation) and the rhombohedral phases (with [111] polarisation)³¹. In this connecting phase, the polarisation has the freedom to align anywhere on the {110} mirror plane between the pseudocubic [111] and [001] directions, giving rise to the high piezoelectric response^{31,45,46}.

Here in $SnTiO_3$, the pronounced existence of the Cm phase and the second triple point, which plays a similar role of bridging the tetragonal phase (with [001] polarisation) and the orthorhombic phase (with [110] polarisation), may also enable high performance, following the pattern of the universal phase diagram discussed in Ref.^{45,46}. The reason is similar to that of $Pb(Zr_{1-x}, Ti_x)O_3$: in this region, polarisation anisotropy nearly vanishes and thus polarisation rotations are easy³⁸. It is also worth noting that many alkaline niobate perovskites show a polymorphic phase transition⁴⁷ between tetragonal phase and orthorhombic phase, similar to what happens in Fig. 2. The polymorphic behaviour can also lead to high piezoelectricity due to the instability with respect to polarisation rotation⁴⁸. However, the temperature stability of their piezoelectric properties for alkaline niobate perovskites is not as good as $Pb(Zr_{1-x}, Ti_x)O_3$. In addition, the large anisotropy along the whole polymorphic boundary line leads to a larger energy barrier between the two polarisation states (tetragonal and orthorhombic), preventing possible polarisation rotations because the phase coexistence results from the diffusive tetragonal to orthorhombic phase transformation⁴. In $SnTiO_3$, unlike polymorphic phase transition, the Cm phase is associated with a triple point, where a low energy barrier between two ferroelectric phases ($P4mm$ and $Amm2$) may exist that facilitates the polarisation rotation and lattice distortion, leading to high performance. Unfortunately, this triple point is not at room temperature for pure $SnTiO_3$ (which is at ~ 750 K as shown in Fig. 2), and may need to be tuned (e.g by doping). For instance, following the lessons from BCZT, it may be possible to use Pb to substitute Sn and/or Zr to substitute Ti. In this way, $SnTiO_3$ can be taken as the matrix material for designing high performance piezoelectric materials.

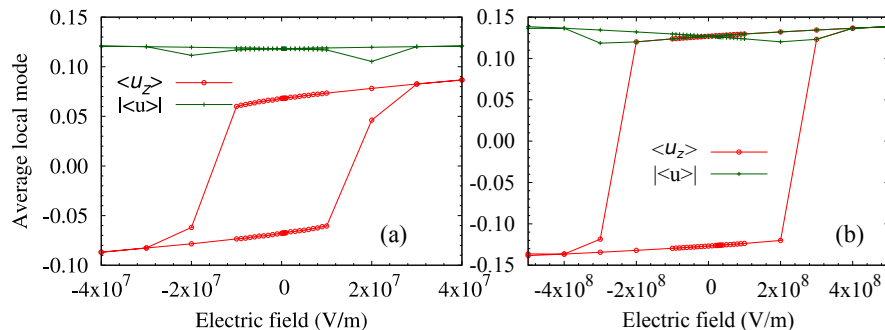


FIG. 3: Hysteresis loop of $SnTiO_3$ at $s = 0.75\%$ (a) and $s = 0\%$ (b) at 300 K. The electric field is applied along the z -axis.

To show that the polarisation in the Cm phase is indeed easy to rotate, we also obtained the hysteresis loop at different epitaxial strains. As Fig. 3 shows, the Cm phase has a

strong effect on the hysteresis loop of $SnTiO_3$. When the Cm phase exists [Fig. 3(a)] at $s = 0.75\%$, the coercive field is $\sim 1.6 \times 10^7$ V/m, reduced by a factor of 10 compared to the

sult obtained when $s = 0\%$ ($> 2 \times 10^8 \text{V/m}$, see Fig. 3(b)). In analogous to magnetic materials, by applying a proper strain (e.g., 0.75%), SnTiO_3 become “soft” ferroelectrics. Interestingly, in the whole process, the magnitude of the polarisation P is approximately a constant [dark green line in Fig. 3], making the whole process a rotation as well as switching of polarisation (albeit a sudden rotation), consistent with previ-

ous computation^{25,26}.

B. Results from direct *ab initio* computation

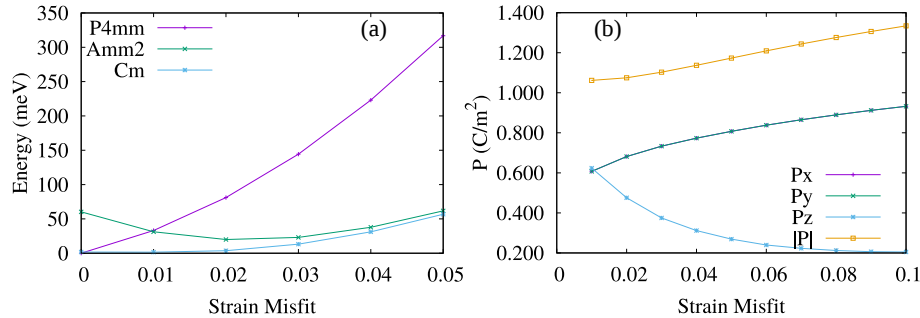


FIG. 4: (a) Energy and polarisation versus strain for three different phases $Amm2$, $P4mm$, and Cm . At $s = 0\%$; (b) The polarisation versus strain for the Cm phase.

To corroborate results obtained from effective-Hamiltonian-based computation, we also obtained numerical results from direct *ab initio* computation. Figure 4(a) shows the energy versus strain for the $P4mm$, $Amm2$, and Cm phases. These phases all appear in the phase diagram of SnTiO_3 (Fig. 2). For a large range of epitaxial strain, the Cm phase has the lowest energy. At $s = 1\%$, the energy of the Cm phase is approximately 29.4 meV lower than that of $P4mm$ or $Amm2$. Such results indicate that the Cm phase can be the ground state for a restricted range of strain, which supports our effective Hamiltonian results. The reason that the Cm phase appears at $s = 0.5\%$ is likely due to the fact that, at this point, the three phases (Cm , $P4mm$, and $Amm2$) have similar energies, and macroscopically the average of $P4mm$ and $Amm2$ also give rise to the Cm phase. On the other hand, when $s > 1\%$, $P4mm$ is no longer an option as its energy becomes much higher than the other two. As the energy difference continue to be smaller with strain, the Cm phase can only exist at low temperature, and eventually disappears. We also note that the Cm phase rarely appear in pure perovskites, whether it is epitaxially strained or not, and SnTiO_3 seems to be an important exception. Figure 4(b) plots the polarisation versus strain for the Cm phase, which is similar to the results obtained in Ref.¹⁷, showing that P_z increases while $P_{x,y}$ decreases with increasing epitaxial strain. We finally note that, despite many attempts, no structural phases involving oxygen octahedron tilting were found to be the ground state. For $0\% < s < 5\%$, structural

phases without oxygen octahedron tilting are consistently more stable in terms of energy.

IV. CONCLUSION

Using effective Hamiltonian based Monte Carlo simulations, we have investigated epitaxially strained SnTiO_3 , found their structural phases at finite temperatures, and obtained its phase diagram with respect to temperature and strain misfit. The phase diagram of SnTiO_3 turns out to be rather complicated, containing two triple points and boundaries that separate ferroelectric phases. Such special features provide unique opportunities to design novel high-performance ferroelectric materials using SnTiO_3 as the matrix, in which the rarely seen Cm phase can exist. In addition, while phonon calculation had shown that AFD related modes are unstable¹⁷, no AFD patterns were found in our simulations, which is likely due to the strong competition from unstable polar modes.

We thank Drs Hongjun Ye, Xiaoyong Wei, and Laurent Bellaiche for fruitful discussion. This work is financially supported by the National Natural Science Foundation of China (NSFC), Grant No. 11574246, 51390472, U1537210, and National Basic Research Program of China, Grant No. 2015CB654903. L.L. acknowledges NSFC Grant No. 11564010 and the Natural Science Foundation of Guangxi (GA139008).

- * Electronic address: dawei.wang@mail.xjtu.edu.cn
† Electronic address: 2009011@glut.edu.cn
- ¹ Xu R J, Liu S, Grinberg I, Karthik J, Damodaran A R, Rappe A M and Martion L W 2015 *Nature Mater.* **14** 79
 - ² Jaffe B, Cook W R and Jaffe H 1971 *Piezoelectric Ceramics* (London: Academic)
 - ³ Saito Y, Takao H, Tani T, Nonoyama T, Takatori K, Homma T, Nagaya T and Nakamura M 2004 *Nature* **432** 84
 - ⁴ Liu W F and Ren X B 2009 *Phys. Rev. Lett.* **103** 257602
 - ⁵ Jaffe B, Roth R S and Marzullo S 1954 *J. Appl. Phys.* **25** 809
 - ⁶ Wessels B W 2007 *Ann. Rev. Mater. Res.* **37** 659
 - ⁷ Ramesh R and Spaldin N A 2007 *Nat. Mater.* **6** 21
 - ⁸ Hwang H Y, Iwasa Y, Kawasaki M, Keimer B, Nagaosa N and Tokura Y 2012 *Nature Mater.* **11** 103
 - ⁹ Yamada H, Ogawa Y, Ishii Y, Sato H, Kawasaki M, Akoh H and Tokura Y 2004 *Science* **305** 646
 - ¹⁰ Ohtomo A and Hwang H Y 2004 *Nature* **427** 423
 - ¹¹ Spaldin N A and Fiebig M 2005 *Science* **309** 391
 - ¹² Wang L, Ju S, You L, Qi Y J, Guo Y W, Ren P, Zhou Y and Wang J L 2015 *Sci. Rep.* **5** 18707
 - ¹³ He F Z, Wells B O, Ban Z G, Alpay S P, Grenier S, Shapiro S M, Si W D, Clark A and Xi X X 2004 *Phys. Rev. B* **70** 235405
 - ¹⁴ Wu J, Xiao D and Zhu J 2015 *Chem. Rev.* **115** 2559
 - ¹⁵ Armiento R, Kozinsky B, Fornari M and ceder G 2011 *Phys. Rev. B* **84** 014103; Matar S, Baraille I and Subramanian M 2009 *Chem. Phys.* **355** 43
 - ¹⁶ Lebedev A I 2009 *Phys. Solid State* **51** 362
 - ¹⁷ Parker W D, Rondinelli J M and Nakhmanson S M 2011 *Phys. Rev. B* **84** 245126
 - ¹⁸ Xie Y H, Yin S, Hashimoto T, Kimura H and Sato T 2009 *J. Mater. Sci.* **44** 4834
 - ¹⁹ Bennett J W, Grinberg I, Davies P K and Rappe A M 2011 *Phys. Rev. B* **83** 144112
 - ²⁰ Suzuki S, Honda A, Iwaji N, Higai S, Ando A, Takagi H, Kasatani H and Deguchi K 2012 *Phys. Rev. B* **86** 060102
 - ²¹ Laurita G, Page K, Suzuki S and Seshadri R 2015 *Phys. Rev. B* **92** 214109
 - ²² Taib M F M, Yaakob M K, Hassan O H and Yahya M Z 2013 *Integr. Ferroelectr.* **142** 119
 - ²³ Taib M F M, Yaakob M K, Badrudin F W, Kudin T I T, Hassan O H and Yahya M Z A 2014 *Integr. Ferroelectr.* **459** 134
 - ²⁴ Uratani Y, Shishidou T and Oguchi T 2008 *Jpn. J. Appl. Phys.* **47** 7735
 - ²⁵ Zhang R Z, Wang D W, Li F, Ye H J, Wei X Y and Xu Z 2013 *Appl. Phys. Lett.* **103** 062905
 - ²⁶ Zhang R Z, Wang D W, Zhu X H, Ye H J, Wei X Y and Xu Z 2014 *J. Appl. Phys.* **116** 174101
 - ²⁷ Zhong W, Vanderbilt D and Rabe K M 1994 *Phys. Rev. Lett.* **73** 1861; 1995 *Phys. Rev. B* **52** 6301
 - ²⁸ H J Ye, Wang D W, Jiang Z J, Cheng S and Wei X Y 2016 *Acta Phys. Sin.* **65** 237101
 - ²⁹ Nishimatsu T, Iwamoto M, Kawazoe Y, and Waghmare U V 2010 *Phys. Rev. B* **82** 134106
 - ³⁰ Vanderbilt D and Cohen M H 2001, *Phys. Rev. B* **63** 094108
 - ³¹ Kornev I A, Bellaiche L, Janolin P E, Dkhil B and Suard E 2006 *Phys. Rev. Lett.* **97** 157601
 - ³² Ye H J, Zhang R Z, Wang D W, Cui Y, Wei J, Wang C L, Xu Z, Qu S B and Wei X Y 2013 *Int. J. Mod. Phys. B* **27** 1350144
 - ³³ Gonze X, Beuken J M, Caracas R, Detraux F, Fuchs M, Rignanese G M, Sindic L, Verstraete M, Zerath G, Jollet F, Torrent M, Roy A, Mikami M, Ghosez P, Raty J Y and Allan D C 2002 *Comp. Mat. Sci.* **25** 478
 - ³⁴ Perdew J P and Wang Y 1992 *Phys. Rev. B* **45** 13244
 - ³⁵ Blöchl P E 1994 *Phys. Rev. B* **50** 17953
 - ³⁶ Garrity K F, Bennett J W, Rabe K M and Vanderbilt D 2014 *Comput. Mater. Sci.* **81** 446
 - ³⁷ Monkhorst H J and Pack J D 1976 *Phys. Rev. B* **13** 5188
 - ³⁸ Zhang N, Yokota H, Glazer A M, Ren Z, Keen D A, Keeble D S, Thomas P A and Ye Z G 2014 *Nat. Commun.* **5** 5231
 - ³⁹ Lu X, Zheng L, Li H and Cao W 2015 *J. Appl. Phys.* **117** 134101
 - ⁴⁰ Liu H, Chen J, Fan L, Ren Y, Pan Z, Lalitha K. V., Rödel J and Xing X, 2017 *Phys. Rev. Lett.* **119**, 017601
 - ⁴¹ Schlom D G, Chen L Q, Eom C B, Rabe K M, Streiffer S K and Triscone J M 2007 *Annu. Rev. Mater. Res.* **37** 589
 - ⁴² Jiang Z J, Zhang R Z, Wang D W, Sichuga D, Jia C L and Bellaiche L 2014 *Phys. Rev. B* **89** 214113
 - ⁴³ Xue D Z, Zhou Y M, Bao H X, Gao J H, Zhou C and Ren X B 2011 *Appl. Phys. Lett.* **99** 122901
 - ⁴⁴ Liu L J, Zheng S Y, Huang Y M, Shi D P, Wu S S, Fang L, Hu C Z and Elouadi B 2012 *J. Phys. D: Appl. Phys.* **45** 295403
 - ⁴⁵ Guo R, Cross L E, Park S E, Noheda B, Cox D E and Shirane G 2000 *Phys. Rev. Lett.* **84** 5423
 - ⁴⁶ Cox D E, Noheda B, Shirane G, Uesu Y, Fujishiro K and Yamada Y 2001 *Appl. Phys. Lett.* **79** 400
 - ⁴⁷ Liu L J, Huang Y M, Li Y H, Fang L, Dammak H, Fan H Q and Thi M P 2012 *Mater. Lett.* **68** 300
 - ⁴⁸ Wada S, Suzuki S, Noma T, Suzuki T, Osada M, Kakihana M, Park S E, Cross L E and Shroud T R 1999 *Jpn. J. Appl. Phys.* **38** 5505
 - ⁴⁹ We have relaxed the cubic phase ($Pm\bar{3}m$) SnTiO_3 using ABINIT (with settings specified in Sec. II) to obtain the lattice parameter $a = 7.312$ Bohr. This lattice parameter is used as the reference value for specifying the misfit strain.
 - ⁵⁰ We tested various AFD related phases, but found none has lower energy than the corresponding phase without AFD. Exceptions may happen at very large epitaxial strain ($s > 8\%$).